Spin density in partially coherent surface-plasmon-polariton vortex fields

Yahong Chen [1,*] Andreas Norrman [2,3] Sergey A. Ponomarenko [4,5] and Ari T. Friberg [3]

[1] *School of Physical Science and Technology & Collaborative Innovation Center of Suzhou Nano Science and Technology, Soochow University, Suzhou 215006, China*

[2] *Photonics Laboratory, ETH Zurich, CH-8093 Zurich, Switzerland*

[3] *Institute of Photonics, University of Eastern Finland, P.O. Box 111, FI-80101 Joensuu, Finland*

[4] *Department of Electrical and Computer Engineering, Dalhousie University, Halifax, Nova Scotia B3J 2X4, Canada*

[5] *Department of Physics and Atmospheric Science, Dalhousie University, Halifax, Nova Scotia B3H 4R2, Canada*

(Received 28 January 2021; accepted 3 June 2021; published 21 June 2021)

We examine the spin angular momentum (SAM) density associated with the recently introduced [Phys. Rev. A **100**, 053833 (2019)], partially coherent surface-plasmon-polariton (SPP) vortex fields at a metal-air interface. We show that the vortices appearing in such structured SPP fields induce a SAM density both in the interface plane and in the direction normal to the interface. We find that the radial and azimuthal SAM densities are caused solely by the SPP electric-field correlations. However, besides the intrinsic spin component induced by the complex SPP wave vector, the azimuthal SAM density remarkably carries also a spin component created by the elementary SPPs comprising the partially coherent vortex field. The normal SAM density, on the other hand, arises mainly due to the SPP magnetic-field correlations. Our analysis specifically demonstrates that the state of coherence of the partially coherent SPP vortex field plays an essential role in shaping the SAM density distributions. Our findings can find applications to near-field particle manipulation and in spin-based integrated photonic circuit design.

DOI: 10.1103/PhysRevA.103.063511

I. INTRODUCTION

Surface plasmon polaritions (SPPs) have occupied a central position in nanophotonics [1] due to their unique physical properties and broad range of attractive multidisciplinary applications [2]. The SPPs are customarily treated as monochromatic, spatially and temporarily fully coherent fields, but lately the partial coherence associated with polychromatic SPP fields has been recognized as a powerful tool to shape their spatial, temporal, and polarization characteristics [3]. Specially, the paradigm of plasmon coherence engineering [4] allows the tailoring of structured, partially coherent SPP fields with desired spatiotemporal statistical attributes [5,6]. Partially coherent SPP vortex fields, generated by a continuum of radially propagating SPP modes with a prescribed initial phase profile and arbitrary inter-SPP correlations, play a particular role among such newly engineered structured SPP fields [7]. This is because such surface electromagnetic fields carry coherence-modulated orbital angular momentum (OAM) with promise, e.g., for nanoparticle trapping and realization of angular-momentum controlled nanolasers.

At the same time, the spin-orbit interaction phenomena in plasmonic systems have attracted rapidly growing interest [8]. Most spin-orbit interaction studies in plasmonics have focused on the spin (circular polarization) control of the spatial degrees of freedom of SPPs, such as spin-induced phase dislocations and OAM in SPP fields [9,10], spin-controlled unidirectional excitation of plasmonic modes [11,12], and spin-induced plasmonic beam shifts (spin-Hall effect of light) [13,14]. The orbit-to-spin degree of freedom [i.e., an orbitally induced spin angular momentum (SAM)] in plasmonic systems, on the other hand, has received much less attention [15–17]. In fact, only recently did Du and coauthors [15] find that a free-space propagating light beam with OAM can excite a skyrmionlike structure of local SAM density in an SPP vortex field. However, to the best of our knowledge, all the spin-orbit interaction phenomena studied so far in plasmonics have dealt with fully spatially coherent SPPs.

In this paper, we explore the distributions of orbitally induced SAM densities in the recently introduced, structured partially coherent SPP vortex fields. We show that the vortex phases of the excitation light source generate serendipitous spin components in the partially coherent SPP vortex field. In particular, we demonstrate that, distinct from the transverse spin of a single SPP induced by its complex wave vector [18], the SAM density associated with a partially coherent SPP vortex field carries an additional azimuthal spin component created by the correlations among the individual SPP modes that make up the field. We show generally that the SAM densities in the interface plane originate exclusively from the SPP electric-field correlations, whereas the SAM density normal to the interface plane is predominantly produced by the SPP magnetic-field correlations. We further analyze the influence of partial optical coherence in controlling the spatial distributions (and orientations) of the spin associated with the random SPP vortex field. Our work thus unveils uncharted avenues into stochastic plasmonic systems of engineered angular momenta.

This work is organized as follows. In Sec. II, we review the partially coherent SPP vortex field structure and discuss

*yahongchen@suda.edu.cn

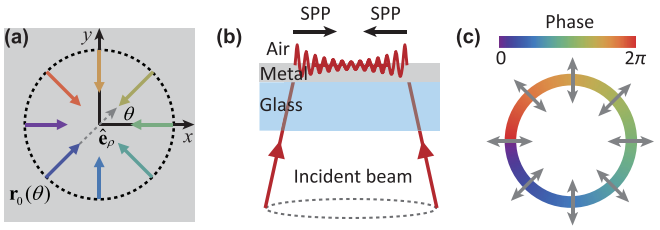

FIG. 1. (a) Synthesis of the partially coherent SPP vortex field by a continuum of radially propagating SPP modes with a prescribed initial phase profile and arbitrary correlations at a metal-air interface. The constituent SPPs are excited at points $\mathbf{r}_0(\theta)$ along a circular ring and propagate toward the ring center in the direction $\hat{\mathbf{e}}_\rho$, where $\theta \in [0, 2\pi)$ is the azimuth angle with respect to the x axis. (b) A focused OAM carrying, radially polarized, and ring shaped, partially coherent incident beam illuminates the glass prism and metal slab structure to excite the radially propagating SPP modes shown in (a). (c) Illustration of the polarization state, beam shape, and phase distribution of a vortex mode with topological charge 1 of the incident partially coherent beam.

its excitation at a metal-air interface. In Sec. III, we derive the analytical expressions for the SAM density of a partially coherent SPP vortex field and assess their implications. In Sec. IV, we examine the role of the state of optical coherence and the associated vortex phases of the excitation light on SAM density modulation. Finally, we summarize our main findings in Sec. V.

II. FIELD STRUCTURE

The partially coherent SPP vortex field can be excited at a metal-air interface ($z = 0$), as depicted in Fig. 1(a), by a continuum of uniformly distributed, partially correlated SPPs, launched at a ring of radius a and propagating toward its center. Each SPP carries an initial phase. Let $0 \leqslant \theta < 2\pi$ be the azimuth angle with respect to the x axis of an SPP at angular frequency ω that is excited at point $\mathbf{r}_0(\theta) = -a\hat{\mathbf{e}}_\rho$ and moving in the direction specified by the unit radial vector $\hat{\mathbf{e}}_\rho = \cos\theta\hat{\mathbf{e}}_x + \sin\theta\hat{\mathbf{e}}_y$, where $\hat{\mathbf{e}}_x$ and $\hat{\mathbf{e}}_y$ are the Cartesian unit vectors in the xy plane. Omitting the time factor $e^{-i\omega t}$, the electric and magnetic fields of such an SPP then read, at point $\mathbf{r}$ in air, as

$$\mathbf{E}(\mathbf{r}, \theta) = E(\theta)\hat{\mathbf{p}}(\theta)e^{i\mathbf{k}(\theta)\cdot[\mathbf{r}-\mathbf{r}_0(\theta)]+i\phi(\theta)}, \tag{1}$$

$$\mathbf{H}(\mathbf{r}, \theta) = \frac{-\kappa_0}{Z_0}E(\theta)\hat{\mathbf{e}}_\theta e^{i\mathbf{k}(\theta)\cdot[\mathbf{r}-\mathbf{r}_0(\theta)]+i\phi(\theta)}. \tag{2}$$

Here $E(\theta)$ is a random amplitude at the excitation point, $\mathbf{k}(\theta) = k_\parallel\hat{\mathbf{e}}_\rho + k_z\hat{\mathbf{e}}_z$ is the SPP wave vector, with $\hat{\mathbf{e}}_z$ being the unit vector along the z axis, while $\hat{\mathbf{p}}(\theta) = \hat{\mathbf{k}}(\theta) \times \hat{\mathbf{e}}_\theta$ and $\hat{\mathbf{e}}_\theta = \hat{\mathbf{e}}_z \times \hat{\mathbf{e}}_\rho$ are the unit normalized polarization vectors of the electric and magnetic fields, respectively, including $\hat{\mathbf{k}}(\theta) = \mathbf{k}(\theta)/|\mathbf{k}|$. The wave-vector magnitude $|\mathbf{k}|$ does not depend on θ and differs from the free-space wave number k_0 [19]. In Eq. (2), $\kappa_0 = k_0/|\mathbf{k}|$ and Z_0 is the free-space impedance. The uniform and nonmagnetic metal film supporting the SPPs is thick enough (e.g., 50–100 nm for Ag [20]) so that mode overlap across the metal layer is negligible, whereupon the tangential and normal SPP wave-vector components are given by [1,21]

$$k_\parallel = k_0\sqrt{\frac{\epsilon_r}{\epsilon_r + 1}}, \quad k_z = k_0\sqrt{\frac{1}{\epsilon_r + 1}}. \tag{3}$$

Above, ϵ_r is the (complex, ω-dependent) relative electric permittivity of the metal. The SPP propagation distance $l_{\mathrm{SPP}} = 1/k_\parallel''$, with the double prime denoting the imaginary part, serves as an upper limit for the ring radius a. Specially, the factor $\phi(\theta)$ in Eqs. (1) and (2) is the initial phase imparted by the illuminating beam to the SPPs at $\mathbf{r}_0(\theta)$ and it generates an SPP vortex phase distribution. The phase difference between any two SPPs obeys [7]

$$\phi(\theta_2) - \phi(\theta_1) = m(\theta_2 - \theta_1), \tag{4}$$

where m is an integer, specified by the topological charge of the exciting source vortex beam.

The correlations among the SPPs are governed by the angular correlation function $W(\theta_1, \theta_2) = \langle E^*(\theta_1)E(\theta_2)\rangle$, where the angle brackets and the asterisk denote ensemble average and complex conjugate, respectively. We assume that the SPP angular correlations are statistically homogeneous [i.e., the angular correlation function depends only on the angular difference, $W(\theta_1, \theta_2) = W(\theta_2 - \theta_1)$] within the 2π range of θ_1 and θ_2, and that each SPP carries the same power. It then follows that [7]

$$W(\theta_1, \theta_2) = I_{\mathrm{SPP}}\sum_{n=-\infty}^{\infty}\beta_n e^{in(\theta_2-\theta_1)}, \tag{5}$$

where I_{SPP} denotes the individual SPP field intensity, n is an integer mode index, and β_n is a Fourier coefficient (i.e., a modal weight). To ensure that $W(\theta_1, \theta_2)$ is a genuine correlation function, β_n should be real and nonnegative. The SPP vortex field is fully coherent if, and only if, the Fourier series in Eq. (5) consists of only one mode. Whenever the series contains more than a single mode the resulting SPP vortex field is partially coherent. In general, as the number of modes in Eq. (5) increases, the SPP vortex field's coherence decreases. In the limiting case of a very large number of modes with identical coefficients (i.e., $\beta_n = 1$), the SPP angular correlation function (effectively) reduces to $W(\theta_1, \theta_2) = 2\pi I_{\mathrm{SPP}}\,\delta(\theta_2 - \theta_1)$, where $\delta(\cdot)$ is the Dirac delta function. The SPPs then are completely uncorrelated and the synthesized SPP vortex fields in any pair of angular directions are mutually uncorrelated.

The phase profile and angular correlation function in Eqs. (4) and (5) of the SPP vortex field can be controlled by using the "plasmon coherence engineering" protocol [4]. As illustrated in Fig. 1(b), this involves a Kretschmann-like setup where the metal film deposited on a glass prism is illuminated by a focused, coherence-engineered, radially polarized beam carrying OAM, whose cross-spectral density matrix before focusing is of the form

$$\mathbf{W}_{\mathrm{in}}(\boldsymbol{\rho}_1, \boldsymbol{\rho}_2) = \sqrt{I(\rho_1)I(\rho_2)}\,\hat{\mathbf{e}}_{\rho_1}^*\hat{\mathbf{e}}_{\rho_2}^{\mathrm{T}}\sum_n \beta_n e^{i(m+n)(\theta_2-\theta_1)}. \tag{6}$$

Here $\boldsymbol{\rho}_1$ and $\boldsymbol{\rho}_2$ are two arbitrary position vectors in the transverse plane of the beam, $I(\rho)$ is its intensity (spectral density) at the radial distance $\rho = (x^2 + y^2)^{1/2}$, with a narrow ring

shape as shown in Fig. 1(c), and T denotes matrix transpose. The incident partially coherent beam can be viewed as an incoherent superposition of a set of completely coherent vortex modes with identical intensity distributions $I(\rho)$ and polarization directions $\hat{\mathbf{e}}_\rho$, but with different topological charges $(m+n)$ and powers β_n. A definite set of β_n coefficients for the angular correlation function in Eq. (5) can be generated through controlling, for instance, by means of a fast modulator such as a digital micromirror device [22], the power of each coherent mode in synthesizing the excitation beam. In practice the so-called perfect vortex beams [23,24] can be used as the fully coherent vortex modes due to their shape independence on the topological charge. Moreover, the spatial degree of coherence of the beam is controlled by the number of modes n and their powers β_n, and its average OAM per photon is given by [25]

$$\boldsymbol{\mathcal{L}}_{\text{in}} = \frac{\sum_n \beta_n (m+n)}{\sum_n \beta_n} \hbar \hat{\mathbf{e}}_z, \tag{7}$$

where $\hbar$ is the reduced Planck constant. After the focusing the beam can be considered as a continuum of inclined TM-polarized plane waves [4], with the SPP coupling optimized by the focusing angle. The SPPs of desired phase profiles and angular correlations ensuing from the illuminated ring at the metal-air surface eventually superpose to form the partially coherent SPP vortex field.

The second-order stochastic properties of the partially coherent SPP vortex field are characterized, at points $\mathbf{r}_1$ and $\mathbf{r}_2$ in air, by means of the electric and magnetic cross-spectral density matrices $\mathbf{W}^{(\text{E})}(\mathbf{r}_1, \mathbf{r}_2) = \langle \mathbf{E}^*(\mathbf{r}_1)\mathbf{E}^{\text{T}}(\mathbf{r}_2)\rangle$ and $\mathbf{W}^{(\text{H})}(\mathbf{r}_1, \mathbf{r}_2) = \langle \mathbf{H}^*(\mathbf{r}_1)\mathbf{H}^{\text{T}}(\mathbf{r}_2)\rangle$ [26,27], where the terms $\mathbf{E}(\mathbf{r}) = \int_0^{2\pi} \mathbf{E}(\mathbf{r}, \theta) d\theta$ and $\mathbf{H}(\mathbf{r}) = \int_0^{2\pi} \mathbf{H}(\mathbf{r}, \theta) d\theta$ are the electric and magnetic field realizations of the SPP vortex field. It then follows from Eqs. (1), (2), (4), and (5) that these two cross-spectral density matrices can be represented via coherent vector modes as [7]

$$\mathbf{W}^{(\text{E})}(\mathbf{r}_1, \mathbf{r}_2) = I_{\text{SPP}} \pi^2 e^{-2k_\parallel'' a} e^{i(k_z z_2 - k_z^* z_1)} \times \sum_n \beta_n \boldsymbol{\mathcal{E}}_n^*(\boldsymbol{\rho}_1) \boldsymbol{\mathcal{E}}_n^{\text{T}}(\boldsymbol{\rho}_2), \tag{8}$$

$$\mathbf{W}^{(\text{H})}(\mathbf{r}_1, \mathbf{r}_2) = \frac{1}{Z_0^2} I_{\text{SPP}} \pi^2 e^{-2k_\parallel'' a} e^{i(k_z z_2 - k_z^* z_1)} \times \sum_n \beta_n \boldsymbol{\mathcal{H}}_n^*(\boldsymbol{\rho}_1) \boldsymbol{\mathcal{H}}_n^{\text{T}}(\boldsymbol{\rho}_2), \tag{9}$$

with the electric and magnetic vector modes reading

$$\begin{aligned} \boldsymbol{\mathcal{E}}_n(\boldsymbol{\rho}) = \{ & -i\kappa_z [\text{J}_{m+n+1}(k_\parallel \rho) - \text{J}_{m+n-1}(k_\parallel \rho)] \hat{\mathbf{e}}_\rho \\ & -\kappa_z [\text{J}_{m+n+1}(k_\parallel \rho) + \text{J}_{m+n-1}(k_\parallel \rho)] \hat{\mathbf{e}}_\theta \\ & + 2\kappa_\parallel \text{J}_{m+n}(k_\parallel \rho) \hat{\mathbf{e}}_z \} e^{i(m+n)\theta}, \end{aligned} \tag{10}$$

$$\begin{aligned} \boldsymbol{\mathcal{H}}_n(\boldsymbol{\rho}) = \{ & \kappa_0 [\text{J}_{m+n+1}(k_\parallel \rho) + \text{J}_{m+n-1}(k_\parallel \rho)] \hat{\mathbf{e}}_\rho \\ & -i\kappa_0 [\text{J}_{m+n+1}(k_\parallel \rho) - \text{J}_{m+n-1}(k_\parallel \rho)] \hat{\mathbf{e}}_\theta \} \\ & \times e^{i(m+n)\theta}. \end{aligned} \tag{11}$$

Here $\kappa_z = k_z/|\mathbf{k}|$, $\kappa_\parallel = k_\parallel/|\mathbf{k}|$, $\text{J}_\nu(\cdot)$ is a Bessel function of the first kind and order ν, and $\hat{\mathbf{e}}_\rho$, $\hat{\mathbf{e}}_\theta$, and $\hat{\mathbf{e}}_z$ form an orthonormal set in cylindrical coordinates.

It is seen from Eqs. (10) and (11) that any SPP vector mode has associated with it a vortex phase $e^{i(m+n)\theta}$. The averaged OAM per photon carried by the partially coherent SPP vortex field is then found to be [7]

$$\boldsymbol{\mathcal{L}} = \frac{\sum_n \xi_n (m+n)}{\sum_n \xi_n} \hbar \hat{\mathbf{e}}_z, \tag{12}$$

where $\xi_n = [\epsilon_0 \xi_n^{(\text{E})} + \mu_0 \xi_n^{(\text{H})}]/4$ is the total electromagnetic energy carried by the SPP vector mode of index n, which corresponds to the topological charge of $(m+n)$. Here, $\xi_n^{(\text{E})} = \beta_n I_{\text{SPP}} \pi^2 e^{-2k_\parallel'' a} \int_V e^{-2k_z'' z} \boldsymbol{\mathcal{E}}_n^{\text{T}}(\boldsymbol{\rho}) \boldsymbol{\mathcal{E}}_n^*(\boldsymbol{\rho}) d^3\mathbf{r}$ and $\xi_n^{(\text{H})} = \beta_n I_{\text{SPP}} \pi^2 e^{-2k_\parallel'' a} \int_V e^{-2k_z'' z} \boldsymbol{\mathcal{H}}_n^{\text{T}}(\boldsymbol{\rho}) \boldsymbol{\mathcal{H}}_n^*(\boldsymbol{\rho}) d^3\mathbf{r}$, with $\int_V \cdot\, d^3\mathbf{r}$ denoting integration over the volume V of the SPP excitation region, are the electric and magnetic parts of an individual mode weight in the coherent mode decomposition of the SPP vortex field. Further, ϵ_0 is the permittivity and μ_0 is the permeability of free space.

We find that the OAM structure of the SPP vortex field in Eq. (12) is akin to that of the incident beam in Eq. (7). In the fully coherent limit, the two averaged OAMs equal $(m+n)\hbar\hat{\mathbf{e}}_z$. However, in a partially coherent scenario, the averaged OAMs of the illumination beam and of the SPP vortex field are not, in general, equal to each other. This is due to the fact that the incident beam's OAM power distribution is determined entirely by β_n, whereas for the SPP vortex field it is specified by ξ_n, which involves β_n and the vector-mode intensity distribution. Even if the OAM of the incident beam vanishes, the partially coherent SPP vortex field may carry a nonzero OAM. For example, if the incident beam of $m = 0$ contains three modes with indices $n = \{-3, 1, 2\}$ and the corresponding $\beta_n = 1$, its averaged OAM is zero. Yet, the averaged OAM of the excited partially coherent SPP vortex field is $\boldsymbol{\mathcal{L}} = [(-3\xi_{-3} + \xi_1 + 2\xi_2)/(\xi_{-3} + \xi_1 + \xi_2)]\,\hbar\hat{\mathbf{e}}_z \neq 0$. Nevertheless, whenever the modal powers satisfy the relation $\beta_n = \beta_{-n-2m}$, i.e., with a symmetric OAM power distribution with respect to zero topological charge, both the incident beam and the excited partially coherent SPP vortex field carry no averaged OAM.

On comparing the vector modes of the partially coherent SPP vortex field in Eqs. (10) and (11) with the electric and magnetic fields of an SPP constituent given by Eqs. (1) and (2), we find that the synthesized vortex field has an additional azimuthal component in its electric field realization and an additional radial component in its magnetic field realization. It follows from the Bessel function properties, namely $\text{J}_{m+n+1}(k_\parallel \rho) + \text{J}_{m+n-1}(k_\parallel \rho) = 2(m+n)(k_\parallel \rho)^{-1} \text{J}_{m+n}(k_\parallel \rho)$, that these extra field components are induced by the topological charge of the vortex phase carried by each vortex mode of the partially coherent incident beam. Hence, the additional components vanish only under the conditions $m+n = 0$ (no vortex carried by a fully coherent incident beam) and $\beta_n = \beta_{-n-2m}$ in the case of a partially coherent incident beam. As we saw above, the latter condition implies that neither the incident beam nor the excited SPP vortex field carry any averaged OAM.

III. SPIN STRUCTURE

The electric and magnetic SAM densities of the partially coherent SPP vortex field at a point $\mathbf{r}$ in air can be assessed

by ensemble averaging over the SAM densities of the (time-averaged) monochromatic field realizations:

$$\mathbf{S}^{(\mathrm{E})}(\mathbf{r}) = \frac{\epsilon_0}{4\omega}\langle \mathbf{E}^*(\mathbf{r}) \times \mathbf{E}(\mathbf{r})\rangle'', \tag{13}$$

$$\mathbf{S}^{(\mathrm{H})}(\mathbf{r}) = \frac{\mu_0}{4\omega}\langle \mathbf{H}^*(\mathbf{r}) \times \mathbf{H}(\mathbf{r})\rangle''. \tag{14}$$

As before, here the double prime stands for the imaginary part, $\mathbf{E}(\mathbf{r}) = \int_0^{2\pi} \mathbf{E}(\mathbf{r},\theta)d\theta$, and $\mathbf{H}(\mathbf{r}) = \int_0^{2\pi} \mathbf{H}(\mathbf{r},\theta)d\theta$. It then follows from Eqs. (1), (2), (4), (5), and (8)–(11) that the above SAM densities of the SPP vortex field can be written in terms of the vector coherent modes as

$$\mathbf{S}^{(\mathrm{E})}(\mathbf{r}) = S_0(z)\left[\sum_n \beta_n \boldsymbol{\mathcal{E}}_n^*(\boldsymbol{\rho}) \times \boldsymbol{\mathcal{E}}_n(\boldsymbol{\rho})\right]'', \tag{15}$$

$$\mathbf{S}^{(\mathrm{H})}(\mathbf{r}) = S_0(z)\left[\sum_n \beta_n \boldsymbol{\mathcal{H}}_n^*(\boldsymbol{\rho}) \times \boldsymbol{\mathcal{H}}_n(\boldsymbol{\rho})\right]'', \tag{16}$$

where $S_0(z) = (4\omega)^{-1}\epsilon_0 I_{\mathrm{SPP}}\pi^2 e^{-2k_\parallel'' a - 2k_z'' z}$. Substituting the electric and magnetic vector modes from Eqs. (10) and (11) into Eqs. (15) and (16), respectively, yields

$$\mathbf{S}^{(\mathrm{E})}(\mathbf{r}) = S_0(z)\left[S_\rho^{(\mathrm{E})}(\boldsymbol{\rho})\hat{\mathbf{e}}_\rho + S_\theta^{(\mathrm{E})}(\boldsymbol{\rho})\hat{\mathbf{e}}_\theta + S_z^{(\mathrm{E})}(\boldsymbol{\rho})\hat{\mathbf{e}}_z\right], \tag{17}$$

$$\mathbf{S}^{(\mathrm{H})}(\mathbf{r}) = S_0(z)S_z^{(\mathrm{H})}(\boldsymbol{\rho})\hat{\mathbf{e}}_z, \tag{18}$$

where the various contributions have the forms,

$$S_\rho^{(\mathrm{E})}(\boldsymbol{\rho}) = 8(\kappa_z\kappa_\parallel^*/k_\parallel)'' \sum_n \beta_n (m+n)|\mathrm{J}_{m+n}(k_\parallel\rho)|^2/\rho, \tag{19}$$

$$\begin{aligned} S_\theta^{(\mathrm{E})}(\boldsymbol{\rho}) = {} & -4(\kappa_z^*\kappa_\parallel)'' \sum_n \beta_n \{\mathrm{J}_{m+n}^*(k_\parallel\rho) \\ & \times [\mathrm{J}_{m+n+1}(k_\parallel\rho) - \mathrm{J}_{m+n-1}(k_\parallel\rho)]\}'' \\ & -4(\kappa_z^*\kappa_\parallel)' \sum_n \beta_n \{\mathrm{J}_{m+n}^*(k_\parallel\rho) \\ & \times [\mathrm{J}_{m+n+1}(k_\parallel\rho) - \mathrm{J}_{m+n-1}(k_\parallel\rho)]\}', \end{aligned} \tag{20}$$

$$S_z^{(\mathrm{E})}(\boldsymbol{\rho}) = -2|\kappa_z|^2 \sum_n \beta_n [|\mathrm{J}_{m+n+1}(k_\parallel\rho)|^2 - |\mathrm{J}_{m+n-1}(k_\parallel\rho)|^2], \tag{21}$$

$$S_z^{(\mathrm{H})}(\boldsymbol{\rho}) = -2\kappa_0^2 \sum_n \beta_n [|\mathrm{J}_{m+n+1}(k_\parallel\rho)|^2 - |\mathrm{J}_{m+n-1}(k_\parallel\rho)|^2]. \tag{22}$$

In the above expressions the prime denotes the real part. Equations (17)–(22) are the key results of this work that lead to several instructive conclusions.

First, the radial and normal spin components $S_\rho^{(\mathrm{E})}(\boldsymbol{\rho})$, $S_z^{(\mathrm{E})}(\boldsymbol{\rho})$, and $S_z^{(\mathrm{H})}(\boldsymbol{\rho})$ are directly produced by the additional contributions induced by the vortex phase into the vector modes comprising the partially coherent SPP vortex field. These spin components are thus closely linked to the vortex phase embedded in the incident light beam. Whenever the incident beam is completely coherent and carries no vortex phase, or if the beam is partially coherent with the modal powers obeying $\beta_n = \beta_{-n-2m}$, then the excited SPP field has neither radial nor normal spin: $S_\rho^{(\mathrm{E})}(\boldsymbol{\rho}) = S_z^{(\mathrm{E})}(\boldsymbol{\rho}) = S_z^{(\mathrm{H})}(\boldsymbol{\rho}) = 0$. Otherwise these spin components of the SPP vortex field are nonzero and their properties can be engineered via controlling the statistical and OAM characteristics of the illumination.

Second, we find that the radial spin component $S_\rho^{(\mathrm{E})}(\boldsymbol{\rho})$ in Eq. (19) originates exclusively from the electric field. Its existence relies not only on the induced vortex phase but also on the complex SPP wave vector and thus on the evanescent nature of the SPP field: $(\kappa_z\kappa_\parallel^*/k_\parallel)'' \neq 0$. For a free-space propagating or a tightly focused vortex beam with real wave vectors such a radial spin component does not exist (see, e.g., [15,28]).

Third, as shown by Eqs. (21) and (22), both the electric and the magnetic field induce normal spin components. The respective components $S_z^{(\mathrm{E})}(\boldsymbol{\rho})$ and $S_z^{(\mathrm{H})}(\boldsymbol{\rho})$ have the same spatial distribution but different weights that obey $S_z^{(\mathrm{E})}(\boldsymbol{\rho})/S_z^{(\mathrm{H})}(\boldsymbol{\rho}) = |\kappa_z|^2/\kappa_0^2$. This ratio is much smaller than unity for typical plasmonic materials (e.g., Ag and Au at optical frequencies [29]), and thus the normal spin component of the SPP vortex field is mainly due to the magnetic field.

And fourth, the partially coherent SPP vortex field has an azimuthal spin component $S_\theta^{(\mathrm{E})}(\boldsymbol{\rho})$ which is generated solely by the electric field. This component points perpendicular to the propagation direction $\hat{\mathbf{e}}_\rho$ of each SPP constituent, i.e., parallel to the intrinsic transverse spin of a single SPP [18,30]:

$$\mathbf{S}(\mathbf{r},\theta) = 2(\kappa_z^*\kappa_\parallel)''\pi^{-2}S_0(z)e^{-2k_\parallel''(\cos\theta x + \sin\theta y)}\hat{\mathbf{e}}_\theta. \tag{23}$$

The transverse spin arises from the complex nature of the SPP wave vector that renders the electric field elliptically polarized in the propagation plane, with no counterpart for a homogeneous plane wave having a real wave vector. The first term in Eq. (20) of the SPP vortex field, which we denote by $[S_\theta^{(\mathrm{E})}]_1$, is similar to the single SPP transverse spin of Eq. (23) in the sense that $[S_\theta^{(\mathrm{E})}]_1 \sim (\kappa_z^*\kappa_\parallel)''$. But the SPP vortex field carries also another azimuthal spin component, viz., the second term $[S_\theta^{(\mathrm{E})}]_2 \sim (\kappa_z^*\kappa_\parallel)'$ in Eq. (20), not found in the single SPP case of Eq. (23). This term arises from correlations among the SPP modes and vanishes only if the incident beam is fully incoherent. In such a limiting case the entire SAM density of the SPP vortex field is specified by $[S_\theta^{(\mathrm{E})}]_1 = -8(\kappa_z^*\kappa_\parallel)''\mathrm{I}_1(2k_\parallel''\rho)$, where $\mathrm{I}_1(2k_\parallel''\rho)$ is the modified Bessel function of the first kind and of order 1, corresponding to an incoherent superposition of the single SPP transverse spins in Eq. (23). In general, however, the spin component $[S_\theta^{(\mathrm{E})}]_2$ induced by the SPP correlations is nonzero and it can be the dominant term, as we demonstrate in Sec. IV. We notice further that the existence of $[S_\theta^{(\mathrm{E})}]_2$ in Eq. (20) relies entirely on a rigorous treatment which accounts for the physically ever-present metal losses; considering an idealized metal with no absorption results in $(\kappa_z^*\kappa_\parallel)' = 0$ and thereby $[S_\theta^{(\mathrm{E})}]_2 = 0$.

IV. EFFECTS OF COHERENCE

Equations (19)–(22) indicate that the state of optical coherence of the incident light beam can play an important role in controlling the SAM density properties. To demonstrate this, we illustrate in Fig. 2 the spatial distributions of the spin components $S_\rho^{(\mathrm{E})}(\boldsymbol{\rho})$, $S_\theta^{(\mathrm{E})}(\boldsymbol{\rho})$, $S_z^{(\mathrm{E})}(\boldsymbol{\rho})$, and $S_z^{(\mathrm{H})}(\boldsymbol{\rho})$ of the SPP vortex

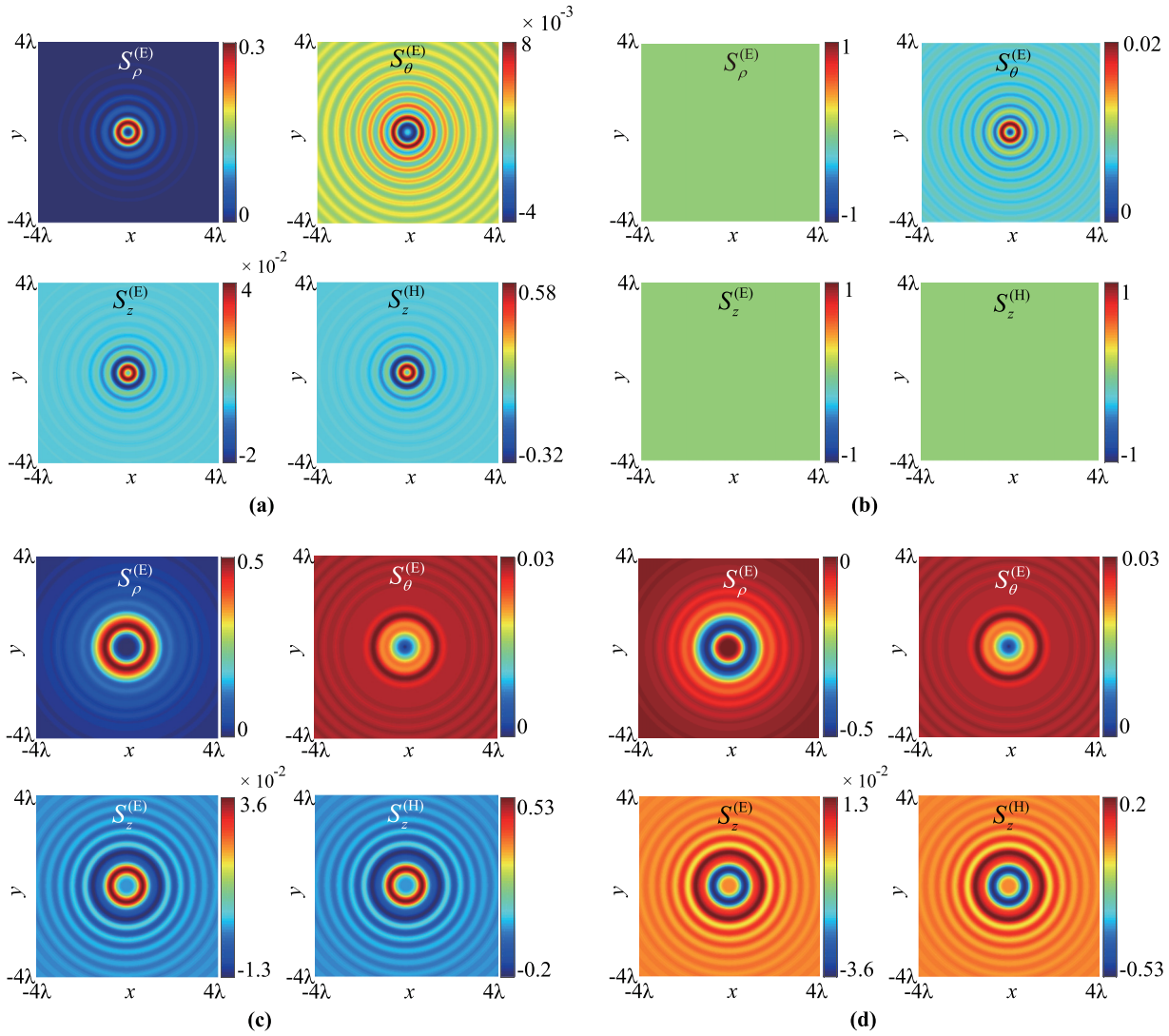

FIG. 2. Spatial distributions of the spin components $S_\rho^{(E)}(\boldsymbol{\rho})$, $S_\theta^{(E)}(\boldsymbol{\rho})$, $S_z^{(E)}(\boldsymbol{\rho})$, and $S_z^{(H)}(\boldsymbol{\rho})$ associated with the partially coherent SPP vortex fields, at an Ag-air interface at free-space wavelength $\lambda = 632$ nm, excited by an incident light beam of varying number of coherent modes and averaged OAM: (a) The incident beam contains a single mode of index $n = 0$ and weight $\beta_0 = 1$, the averaged OAM is $2\hbar$; (b) the incident beam contains three modes of index $n \in \{-3, -2, -1\}$ and the corresponding weights $\beta_n = 1$, the averaged OAM is 0; (c) the incident beam contains 11 modes of index $n \in \{-5, ..., 5\}$ and the corresponding weights $\beta_n = 1$, the averaged OAM is $2\hbar$; (d) the incident beam contains 11 modes of index $n \in \{-9, ..., 1\}$ and the corresponding weights $\beta_n = 1$, the averaged OAM is $-2\hbar$. The topological charge of the incident light beam in all cases is fixed at $m = 2$ and the excitation ring radius a equals the SPP propagation length l_{SPP}. The relative permittivity of Ag is taken from empirical data [29].

fields excited at an Ag-air interface by an incident light beam with a varying number of coherent modes and averaged OAM. The topological charge of the incident beam is fixed at $m = 2$ and the excitation ring radius a equals the SPP propagation length $l_{\mathrm{SPP}} = 1/k_\parallel''$ at the considered free-space wavelength $\lambda = 632$ nm. First of all, in Fig. 2(a) we display the spin components of the SPP vortex field generated by a fully coherent incident beam consisting of a single lowest-order mode with index $n = 0$. The source beam therefore carries a vortex phase $e^{i2\theta}$ and has the average OAM of $2\hbar$ per photon [Eq. (7)]. In this totally coherent case, one observes that the vortex phase indeed creates SAM density terms both parallel and normal to the interface, with the vortex-induced spin components $S_\rho^{(E)}(\boldsymbol{\rho})$ and $S_z^{(H)}(\boldsymbol{\rho})$ being dominant.

Next we consider the spin properties of partially coherent SPP vortex fields by increasing the number of modes. In Fig. 2(b), the source beam contains three coherent modes of indices $n \in \{-3, -2, -1\}$ and of equal weights $\beta_n = 1$. Although the coherent modes individually carry nonzero vortex phases, their incoherent superposition results in a zero averaged OAM both for the incident beam [Eq. (7)] and for the excited SPP field [Eq. (12)]. Therefore, contrary to the fully coherent scenario in Fig. 2(a), for the partially coherent case in Fig. 2(b) the vortex-induced spin components $S_\rho^{(E)}(\boldsymbol{\rho})$, $S_z^{(E)}(\boldsymbol{\rho})$, and $S_z^{(H)}(\boldsymbol{\rho})$ vanish, whereas the azimuthal term $S_\theta^{(E)}(\boldsymbol{\rho})$ becomes dominant. On further decreasing the coherence of the source beam by increasing the number of modes to 11, and taking the mode indices $n \in \{-5, ..., 5\}$

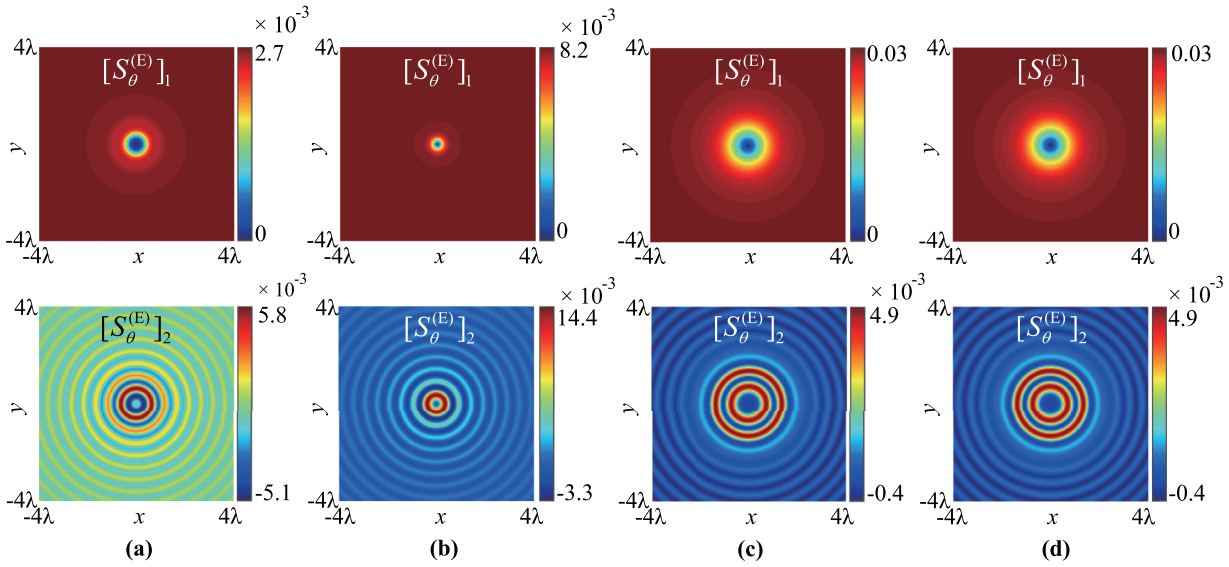

FIG. 3. Spatial distributions of the first term $[S_\theta^{(\mathrm{E})}]_1$ and the second term $[S_\theta^{(\mathrm{E})}]_2$ of the azimuthal spin component $S_\theta^{(\mathrm{E})}(\boldsymbol{\rho})$ in Eq. (20) for the partially coherent SPP vortex fields of Fig. 2.

and $n \in \{-9, ..., 1\}$, we show the associated SAM density behavior in Figs. 2(c) and 2(d), respectively. All the modes carry the same power as before. The averaged OAM of the incident light beams in Figs. 2(c) and 2(d) is $2\hbar$ and $-2\hbar$, respectively, thus having equal magnitude but opposite signs. As observed from Figs. 2(c) and 2(d), the spin components $S_\rho^{(\mathrm{E})}(\boldsymbol{\rho})$, $S_z^{(\mathrm{E})}(\boldsymbol{\rho})$, and $S_z^{(\mathrm{H})}(\boldsymbol{\rho})$ of the SPP vortex fields switch their sign as well, but their azimuthal spin components $S_\theta^{(\mathrm{E})}(\boldsymbol{\rho})$ are independent of the topological charge sign and hence display the same distribution. We note that the specific values for β_n used in Fig. 2 are for illustrative purposes. In general they can be any real numbers in the range $\beta_n \geqslant 0$.

Furthermore, we infer from Fig. 2 that the oscillations in the spatial distribution of $S_\theta^{(\mathrm{E})}(\boldsymbol{\rho})$ gradually decrease with lowering the optical coherence of the incident beam. This behavior can be understood by examining the terms $[S_\theta^{(\mathrm{E})}]_1 \sim (\kappa_z^* \kappa_\parallel)''$ and $[S_\theta^{(\mathrm{E})}]_2 \sim (\kappa_z^* \kappa_\parallel)'$ in Eq. (20), with the former resembling the transverse spin of a single SPP [Eq. (23)] while the latter having no such correspondence. As explained in Sec. III, for a totally incoherent source the individual SPPs do not interfere and the SAM density of the SPP vortex field is entirely due to the first term $[S_\theta^{(\mathrm{E})}]_1 = -8(\kappa_z^* \kappa_\parallel)'' \mathrm{I}_1(2k_\parallel'' \rho)$. Hence, when the degree of optical coherence gets low, the SPP interference is weak and the azimuthal spin component of the SPP vortex field behaves roughly as such a nonoscillating, incoherent superposition of transverse spins of the SPP modes. However, when the coherence of the incident beam increases, the correlations among the SPP modes become stronger and the contribution of the emerging second term $[S_\theta^{(\mathrm{E})}]_2$ to the total azimuthal spin $S_\theta^{(\mathrm{E})}(\boldsymbol{\rho})$ is no longer negligible. Figure 3 illustrates this previously uncharted behavior, from which we observe that for a sufficiently high degree of coherence it is the correlations-induced contribution $[S_\theta^{(\mathrm{E})}]_2$, instead of $[S_\theta^{(\mathrm{E})}]_1$, which becomes the dominant term and produces the spatial oscillation of $S_\theta^{(\mathrm{E})}(\boldsymbol{\rho})$.

V. CONCLUSIONS

We have studied the spatial distribution of the SAM density associated with a partially coherent SPP vortex field excited by a coherence-tailored radially polarized vortex beam at a metal-air interface in the classic Kretschmann-type configuration. We found that such an SPP vortex field possesses spin components both along the interface plane and normal to it and they are all intimately related to the vortex phase carried by each coherent mode of the partially coherent incident light beam. The spin components in the interface plane, both radial and azimuthal, involve only the electric-field correlations, whereas the normal spin component is mostly due to the magnetic-field correlations.

We showed specifically that the radial and normal spin components vanish only in the cases when the incident beam carries no vortex phase or when the incident beam is composed of a set of vortex modes with a symmetric OAM spectrum distribution with respect to the zero topological charge. We also demonstrated that the SPP vortex field displays an azimuthal spin vortex distribution, i.e., it contains an azimuthal spin component with radial symmetry. However, unlike the transverse spin carried by a single SPP, the azimuthal spin of the synthesized SPP vortex field is composed of two parts: a term originating from the complex nature of the SPP wave vector and a previously undiscovered term induced by the electric-field correlations, which can be the dominant contribution in the case of strong interference. Further, we showed that the optical coherence of the incident beam plays an important role in controlling the SAM density distribution of the partially coherent SPP vortex field. In particular, we demonstrated that by adjusting the light source coherence, the vortex phase induced radial and normal spin components can be turned on and off and the spin signs can be switched. Our findings can find applications in plasmonic spin-orbit interactions and optical near-field tweezing [31,32], and they are expected to facilitate further advances in this rapidly developing field.

ACKNOWLEDGMENTS

This research was supported by the National Natural Science Foundation of China (NSFC) (Grant No. 11904247), the Natural Science Foundation of Jiangsu Higher Education Institutions of China (Grant No. 19KJB140017), the Natural Science Foundation of Shandong Province (Grant No. ZR2019QA004), the Jane and Aatos Erkko Foundation (Finland), the Natural Sciences and Engineering Research Council of Canada (Grant No. RGPIN-2018-05497), the Joensuu University Foundation, and the Academy of Finland (Project No. 310511). This work is part of the Academy of Finland Flagship Program "Photonics Research and Innovation" (PREIN Project No. 320166).

[1] L. Novotny and B. Hecht, *Principles of Nano-Optics*, 2nd ed. (Cambridge University, Cambridge, 2012).

[2] S. A. Maier, *Plasmonics: Fundamentals and Applications* (Springer, Berlin, 2007).

[3] Y. Chen, A. Norrman, S. A. Ponomarenko, and A. T. Friberg, Optical coherence and electromagnetic surface waves, Prog. Opt. **65**, 105 (2020).

[4] A. Norrman, S. A. Ponomarenko, and A. T. Friberg, Partially coherent surface plasmon polaritons, EPL **116**, 64001 (2016).

[5] Y. Chen, A. Norrman, S. A. Ponomarenko, and A. T. Friberg, Partially coherent axiconic surface plasmon polariton fields, Phys. Rev. A **97**, 041801(R) (2018).

[6] Y. Chen, A. Norrman, S. A. Ponomarenko, and A. T. Friberg, Coherence lattices in surface plasmon polariton fields, Opt. Lett. **43**, 3429 (2018).

[7] Y. Chen, A. Norrman, S. A. Ponomarenko, and A. T. Friberg, Partially coherent surface plasmon polariton vortex fields, Phys. Rev. A **100**, 053833 (2019). We note that a minus sign is missing in front of Eq. (41) and that the average OAMs $\mathcal{L}(\omega)$ in Figs. 2–4 are the values of the average angular momentum of the incident beam.

[8] K. Y. Bliokh, F. J. Rodríguez-Fortuño, F. Nori, and A. V. Zayats, Spin-orbit interactions of light, Nat. Photonics **9**, 796 (2015).

[9] Y. Gorodetski, A. Niv, V. Kleiner, and E. Hasman, Observation of the Spin-Based Plasmonic Effect in Nanoscale Structures, Phys. Rev. Lett. **101**, 043903 (2008).

[10] Y. Gorodetski, S. Nechayev, V. Kleiner, and E. Hasman, Plasmonic Aharonov-Bohm effect: Optical spin as the magnetic flux parameter, Phys. Rev. B **82**, 125433 (2010).

[11] F. J. Rodríguez-Fortuño, G. Marino, P. Ginzburg, D. O'Connor, A. Martínez, G. A. Wurtz, and A. V. Zayats, Near-field interference for the unidirectional excitation of electromagnetic guided modes, Science **340**, 328 (2013).

[12] D. O'Connor, P. Ginzburg, F. J. Rodríguez-Fortuño, G. A. Wurtz, and A. V. Zayats, Spin-orbit coupling in surface plasmon scattering by nanostructures, Nat. Commun. **5**, 5327 (2014).

[13] K. Y. Bliokh, Y. Gorodetski, V. Kleiner, and E. Hasman, Coriolis Effect in Optics: Unified Geometric Phase and Spin-Hall Effect, Phys. Rev. Lett. **101**, 030404 (2008).

[14] X. Ling, X. Zhou, K. Huang, Y. Liu, C.-W. Qiu, H. Luo, and S. Wen, Recent advances in the spin Hall effect of light, Rep. Prog. Phys. **80**, 066401 (2017).

[15] L. Du, A. Yang, A. V. Zayats, and X. Yuan, Deep-subwavelength features of photonic skyrmions in a confined electromagnetic field with orbital angular momentum, Nat. Phys. **15**, 650 (2019).

[16] S. Tsesses, K. Cohen, E. Ostrovsky, B. Gjonaj, and G. Bartal, Spin–orbit interaction of light in plasmonic lattices, Nano Lett. **19**, 4010 (2019).

[17] Y. Dai, Z. Zhou, A. Ghosh, R. S. K. Mong, A. Kubo, C.-B. Huang, and H. Petek, Plasmonic topological quasiparticle on the nanometre and femtosecond scales, Nature (London) **588**, 616 (2020).

[18] K. Y. Bliokh and F. Nori, Transverse spin of a surface polariton, Phys. Rev. A **85**, 061801(R) (2012).

[19] A. Norrman, T. Setälä, and A. T. Friberg, Long-range higher-order surface-plasmon polaritons, Phys. Rev. A **90**, 053849 (2014).

[20] A. Norrman, T. Setälä, and A. T. Friberg, Surface-plasmon polariton solutions at a lossy slab in a symmetric surrounding, Opt. Express **22**, 4628 (2014).

[21] A. Norrman, T. Setälä, and A. T. Friberg, Exact surface-plasmon polariton solutions at a lossy interface, Opt. Lett. **38**, 1119 (2013).

[22] X. Zhu, J. Yu, Y. Chen, F. Wang, O. Korotkova, and Y. Cai, Experimental synthesis of random light sources with circular coherence by digital micro-mirror device, Appl. Phys. Lett. **117**, 121102 (2020).

[23] P. Li, Y. Zhang, S. Liu, C. Ma, L. Han, H. Cheng, and J. Zhao, Generation of perfect vectorial vortex beams, Opt. Lett. **41**, 2205 (2016).

[24] X. Wang, Y. Zhang, Y. Dai, C. Min, and X. Yuan, Enhancing plasmonic trapping with a perfect radially polarized beam, Photonics Res. **6**, 847 (2018).

[25] Y. Zhang, Y. Cai, and G. Gbur, Control of orbital angular momentum with partially coherent vortex beams, Opt. Lett. **44**, 3617 (2019).

[26] L. Mandel and E. Wolf, *Optical Coherence and Quantum Optics* (Cambridge University, Cambridge, 1995).

[27] A. T. Friberg and T. Setälä, Electromagnetic theory of optical coherence (invited), J. Opt. Soc. Am. A **33**, 2431 (2016).

[28] M. Li, Y. Cai, S. Yan, Y. Liang, P. Zhang, and B. Yao, Orbit-induced localized spin angular momentum in strong focusing of optical vectorial vortex beams, Phys. Rev. A **97**, 053842 (2018).

[29] E. D. Palik, editor, *Handbook of Optical Constants of Solids* (Academic Press, Orlando, 1998).

[30] K. Y. Bliokh and F. Nori, Transverse and longitudinal angular momenta of light, Phys. Rep. **592**, 1 (2015).

[31] A. Ivinskaya, N. Kostina, A. Proskurin, M. I. Petrov, A. A. Bogdanov, S. Sukhov, A. A. Krasavin, A. Karabchevsky, A. S. Shalin, and P. Ginzburg, Optomechanical manipulation with hyperbolic metasurfaces, ACS Photonics **5**, 4371 (2018).

[32] Y. Zhang, C. Min, X. Dou, X. Wang, H. P. Urbach, M. G. Somekh, and X. Yuan, Plasmonic tweezers: for nanoscale optical trapping and beyond, Light: Sci. Appl. **10**, 59 (2021).